Proceedings World Geothermal Congress 2020+1
Reykjavik, Iceland, April - October 2021

Drillability of Granitic Rocks After Thermal Loading

Ruben Bjørge[1], Ahmad Mardoukhi[2], Mikko Hokka[2], Filip Dahl[3] and Alexandre Kane[1]

[1]SINTEF Industry, Trondheim, Norway, [2]Tampere University, Tampere, Finland, [3]SINTEF Community, Trondheim, Norway

ruben.bjorge@sintef.no, ahmad.mardoukhi@tuni.fi, mikko.hokka@tuni.fi, Pascal-Alexandre.Kane@sintef.no

Keywords: drilling, granite, non-mechanical drilling

ABSTRACT

Balmoral Red granite and Kuru Grey granite were exposed to heat shock using a stationary flame torch and a moving plasma gun. The effect of the heat shock on the drillability was quantified using the Sievers' J-miniature drill test. The samples were also investigated using X-ray micro-computed tomography and scanning electron microscopy. The flame torch created mainly surface porosity in the Kuru Grey granite, but the drillability did not increase. A larger number of cracks were found in the flame torched Balmoral Red granite, and here the drillability increased significantly where the heat input was greatest. The plasma gun caused spallation of the surface in both granite types, and an increase in drillability in a damage layer 100-200 µm thick.

1. INTRODUCTION

Geothermal energy seeks to harvest heat from rock formations as deep as 5 km, with a view to using deeper formations in the future (Tomac and Sauter 2018). The high cost of drilling deep wells in hard rock formations is a significant bottleneck for the realization of widespread exploitation of deep geothermal energy. Percussive drilling is considered the most effective drilling technique in hard rock (Mardoukhi et al. 2017b). Several rock breaking technologies have been developed over the years to increase the drilling efficiency further, such as water-jet assisted drilling (Hood 1976). There are also techniques using heat to break the rock, such as flame-jet thermal spallation drilling (Rauenzahn and Tester 1989).

Mardoukhi et al. looked instead at the effect of weakening the rock using thermal loading on the rock strength (Mardoukhi et al. 2017a, b, c, 2018). Using liquid penetrant optical microscopy, they could relate changes in the rock surface induced by the thermal loading to rock tensile strength. The tensile strength was measured under dynamic conditions using a split Hopkinson pressure bar, and under quasi-static conditions. In this study, we instead make use of the Sievers' J miniature drill test to measure the drillability of the rock before and after thermal loading.

2. METHODS

Two types of granitic rock were used in this study: Balmoral Red and Kuru Grey. The mineralogical content of the two types of rock is shown in Table 1. The Balmoral Red granite has much larger grains than Kuru Grey granite.

Table 1: Mineral composition of the granites used in this study.

Kuru Grey granite (Fourmeau et al. 2014)		Balmoral Red granite (Mardoukhi et al. 2017b)	
Mineral	Weight percent	Mineral	Weight percent
Quartz	35.3	Potash feldspar	40
Albite intermediate	30.4	Quartz	33
Microcline maxi	28.0	Plagioclase	19
Biotite	2.9	Biotite and hornblende	8
Diopside	2.1		
Chlorite IIb	1.3		

2.1 Thermal loading

Two types of thermal loading of the rock surface were performed: flame torch and plasma shock. For the flame torch, disc samples were used with a diameter of 40.5 mm and thickness 21 mm for the Balmoral Red, and a diameter of 41 mm and thickness 16 mm for the Kuru Grey. The samples were kept stationary at a fixed distance from the tip of an oxygen-acetylene flame for 60 seconds. Samples were air-cooled after exposure.

For the plasma shock, a 50 kW plasma gun was moved across the surface of rock slabs at a fixed distance of 6.5 cm from the rock surface. Speeds of 50, 75 and 100 mm/s were used. Samples were cooled in air after exposure.

2.2 Sievers' drillability test

The Sievers' J-miniature drill test is typically used to give a measure of the rock surface hardness or resistance to indentation (Sievers 1950; Dahl et al. 2007). It was chosen in this work due to the small sample size needed and to investigate the depth of any weakening caused by the thermal loading. SJ is defined as the mean value of the measured drillhole depth in tenths of a millimetre, after 200 revolutions of an 8.5 mm tungsten carbide drill bit rotating at 180 RPM. Therefore, the higher the SJ value, the greater the drillability of the rock sample. Normally, 4-8 drillings are performed, depending on variations in the texture of the sample. The setup used logs the penetration depth as a function of time, with a sampling rate of 10 Hz.

2.3 Characterization

X-ray micro-computed tomography (μ-CT) was performed using a Nikon XTH 225 scanner. Polychromatix X-rays from a Wolfram anode using an acceleration voltage of 165 kV and an anode current of 160 A was used with an exposure time of 1000 ms per projection image. Scanning electron microscopy (SEM) was performed using Hitachi S-3400N and Hitachi SU-6600 SEMs. Both secondary electron (SE) and backscattered electron (BSE) modes were used to provide either topographical or atomic-number contrast, respectively.

3. RESULTS AND DISCUSSION

3.1 Sievers' miniature drilling test

The SJ values obtained for the tested samples are plotted in Figure 1. The reference (i.e., unexposed) samples had an SJ value of 4.5±1.1 mm/10 (standard error) for Balmoral Red and 3.7±0.4 mm/10 for Kuru Grey. The larger spread in the values for Balmoral Red is due to the large grain size in this rock type compared to the size of the drill bit, and the different mechanical properties of the different minerals present in the rock.

The Kuru Grey granite does not show a large difference between the reference sample and the exposed samples: the plasma shocked samples have a slightly higher SJ value, while the flame torched samples have a slightly lower SJ value. A decrease in drillability after thermal loading is unexpected but could be due to the release of stresses during exposure. Alternatively, the decrease in drillability for the flame-torched samples reflects the variance between different samples of Kuru Grey.

The Balmoral Red granite is different in that two conditions show a significant increase in drillability after thermal loading: the most severely plasma shocked sample (50 mm/s) and the centre of the flame torched samples. The plasma shock 50 sample shows a large scatter in values. This is due to the large grain size, and difference between the different minerals in how they respond to the thermal loading. The flame torched sample showed no significant increase in drillability away from the centre of the disc, but a considerable increase in drillability in the centre, where the thermal loading was highest. Unfortunately, the number of measurements for the centre of the discs was limited to two. This means that the average might be inaccurate, but still it shows that at least some of the minerals have been weakened by the flame torch.

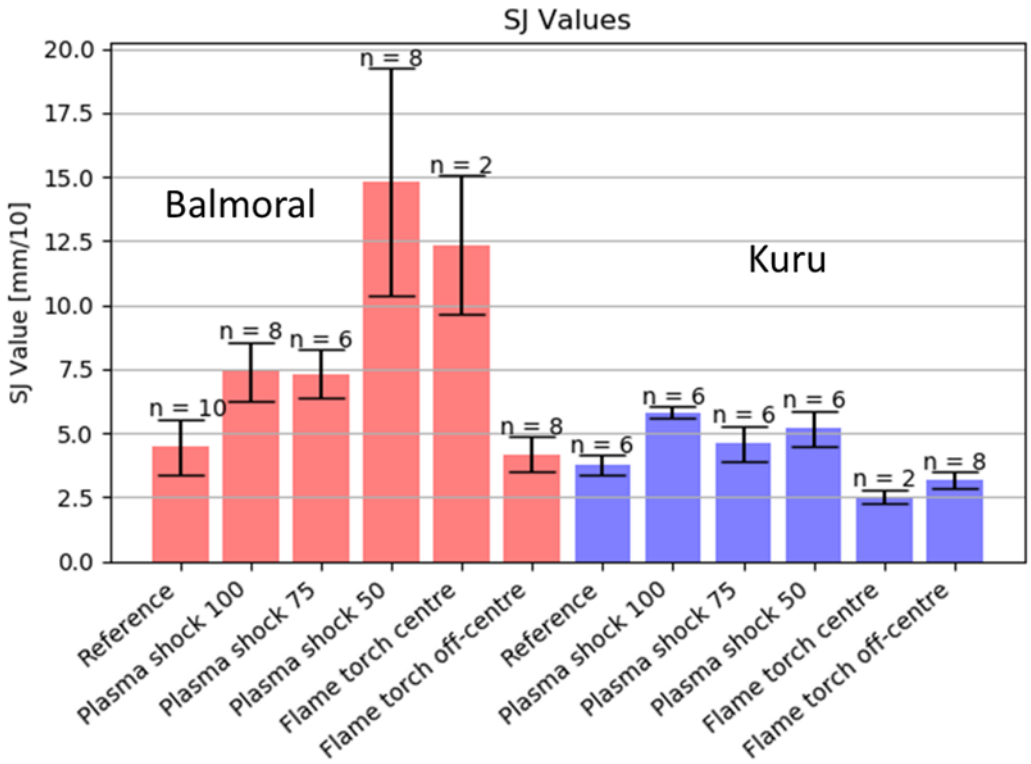

Figure 1: SJ values for tested rock samples: Balmoral Red (left) and Kuru Grey (right). Error bars correspond to standard error. The number of drill tests per condition is indicated.

Although the SJ value (i.e., the final penetration depth) is a valuable indicator of surface hardness, useful information can also be obtained from plotting the average penetration depth as a function of time for each thermal load condition (Figure 2). For most of the curves there is a clear break after the first few seconds. This is due to dulling of the drill bit and is a common feature of the SJ miniature drill test applied to hard rocks. For the Kuru Grey, we see a large initial increase in penetration depth, followed by a slow increase in depth for the remainder of the test. The slope of the curves is nearly the same for all the samples after the initial phase, the main difference between the samples occurs in the first 5-10 seconds. The only exception is the Plasma shock 100 sample, which has a slightly higher rate of penetration throughout the test.

For the Balmoral Red granite, the four samples with lowest drillability are similar to the Kuru Grey in the presence of a clear break in the curve and similar slope after an initial rapid increase in penetration depth. The samples with the highest SJ values (plasma shock 50 and flame torch centre) differ in that there is not a clear break, but instead the slope (i.e., the rate of penetration) decreases more gradually. This suggests that these two samples have been affected by the thermal loading to a greater depth than the other samples.

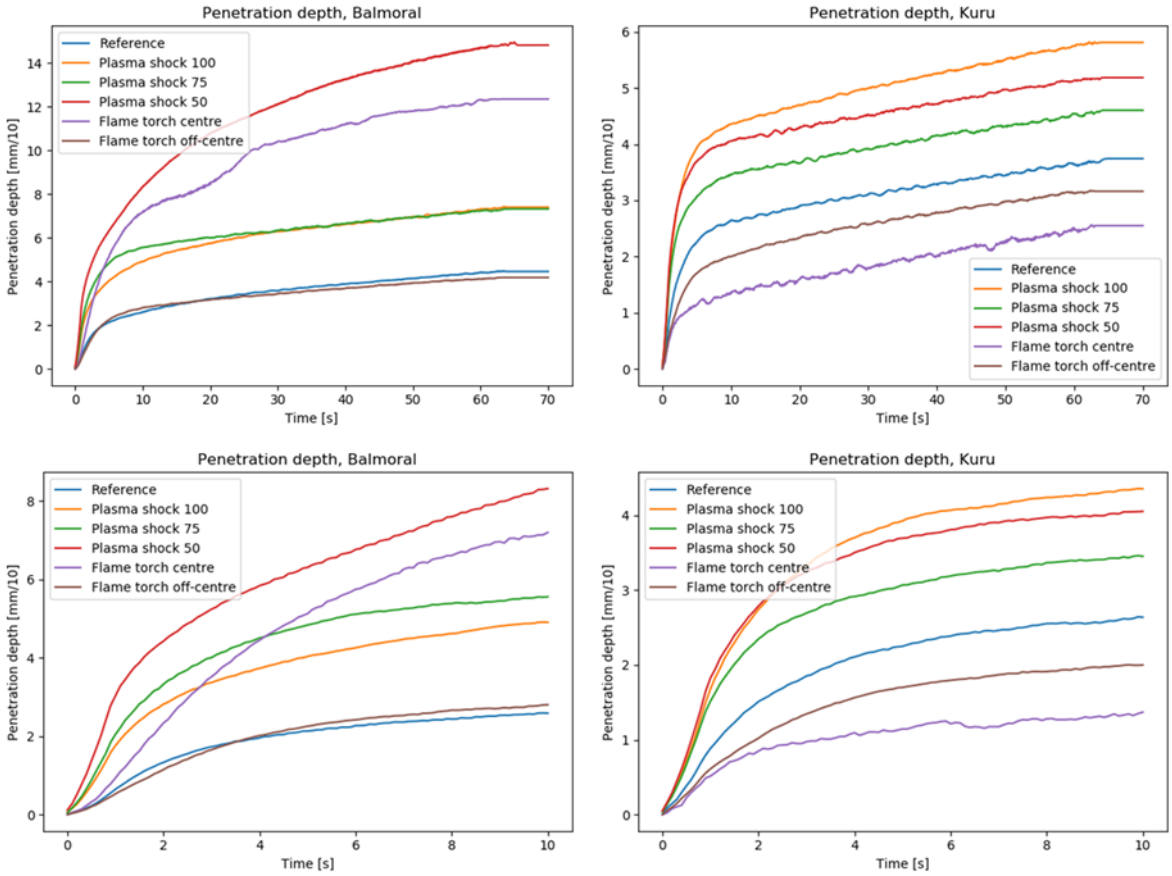

Figure 2: Plots of average penetration depth versus time for Kuru Grey granite (left) and Balmoral Red granite (right). The top plots show the entire duration of the tests, while the bottom plots show the first 10 seconds.

Since most of the conditions are only different during an initial phase of the drill test, we plot the average penetration depth during the first 10 seconds of the drill test in the bottom half of Figure 2. Considering the Kuru Grey granite, we see that the slope of the curves, i.e., the rate of penetration (ROP), is roughly identical for all samples after approximately six seconds. However, in the first few seconds, the ROP is higher for the plasma shocked samples compared to the reference and flame torched samples. This suggests that the drillability of the plasma shocked samples is increased in a thin surface layer, around 100-200 µm thick. This could be due to an increased porosity of the surface due to thermal spallation, as discussed later.

The Balmoral Red granite shows a similar trend in that the plasma shocked samples have an initial ROP that is higher than for the reference sample. Plasma shock 75 and 100 decrease to the same rate of penetration as the reference sample after approximately six seconds. The ROP for the two samples with highest drillability does not decrease to the level of the others until towards the end of test, but it is interesting to note the difference in the evolution of the ROP for these two samples. The plasma shock 50 sample has a high initial ROP, while the flame torched sample has a lower initial ROP that decreases quite slowly compared to the other samples. The difference could be due to different distributions of damage caused by the different types of thermal loading.

To consider the behaviour during the beginning of the drill test, we plot the time to reach a depth of 100 µm in Figure 3. This also allows us to consider the scatter in the measurements. For both types of granite, the average time to reach 100 µm is on average less for the plasma shocked samples than for the reference sample. However, the spread in values for the reference samples is so large that they overlap with the plasma shocked samples. The plasma shock treatment reduces the variance in the time to penetrate the first 100 µm of the samples. Similar results were obtained when considering the time to reach a depth of 200 µm.

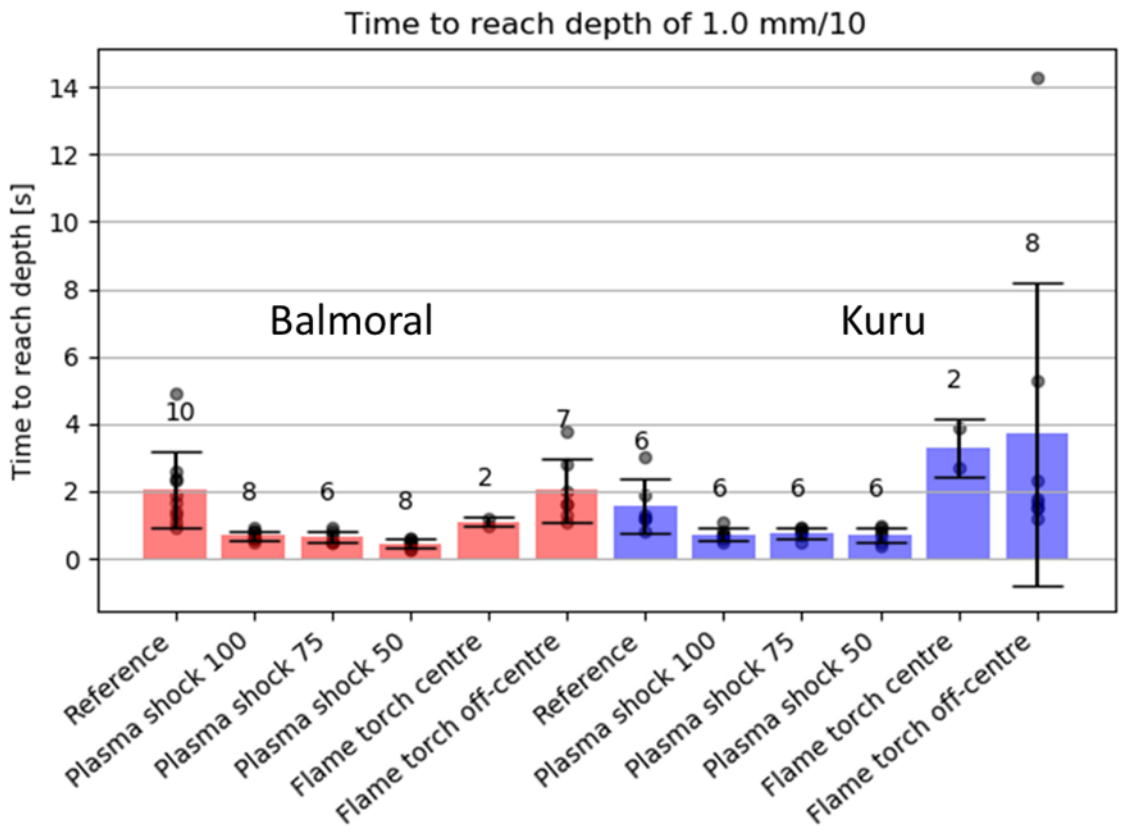

Figure 3: Time to reach a penetration depth of 100 µm for the tested rock samples. Error bars correspond to standard deviation. Individual measurements are indicated by dots. Numbers indicate the number of measurements.

3.2 SEM

SEM gives an overview of the effect of the thermal loading on the sample surface. Typical SEM images of the centre of the flame torched samples are shown in Figure 4. For the Kuru Grey, there is a large amount of surface porosity. This is most visible from the dark contrast in the BSE image. There are also some cracks present. For the coarse-grained Balmoral Grey, the flame torched sample contained large cracks on the surface (width approximately 50 µm). This corresponds well with liquid penetrant optical microscopy results previously reported (Mardoukhi et al. 2017b, a).

SEM images of the plasma shocked granite samples are shown in Figure 5. Only the 50 mm/s and 100 mm/s samples are shown. In these sample the thermal loading has led to spallation of the surface positioned under the path of the plasma gun. Areas outside the path of the gun are not spalled. A noticeable feature of the spalled areas, compared with the unexposed areas, is the presence of areas that appear smooth and dark in the secondary electron images. EDX mapping showed that these are quartz grains. There are also some cracks in the plasma shocked Balmoral Red granite.

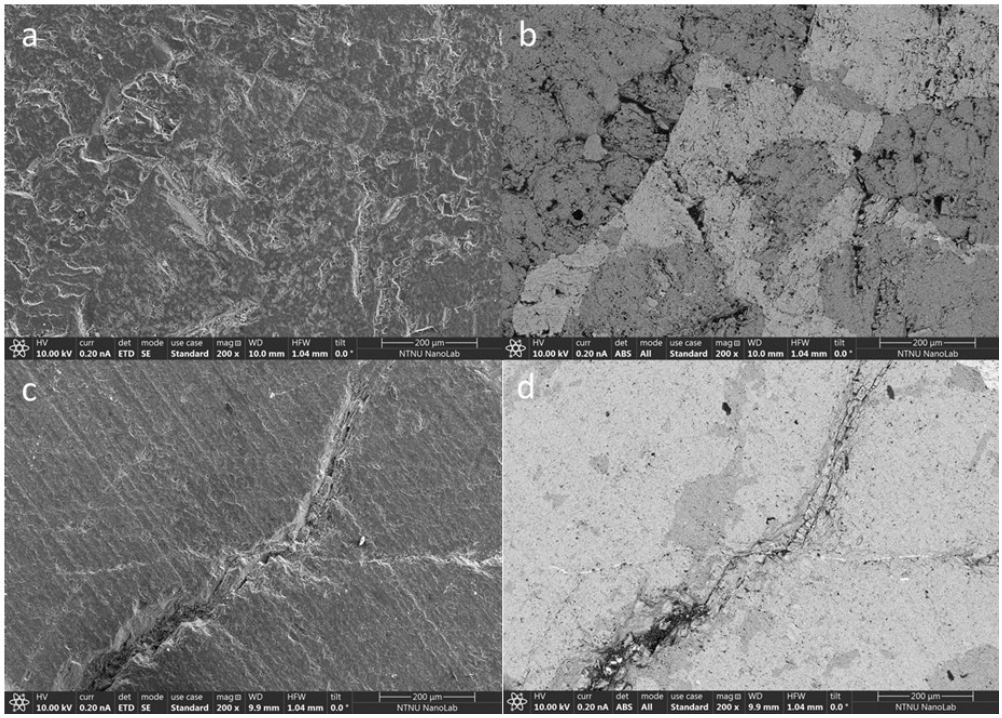

Figure 4: SEM images of flame torched granite samples: (a) Kuru Grey SE image (b) Kuru Grey BSE image (c) Balmoral Red SE image (d) Balmoral Red BSE image.

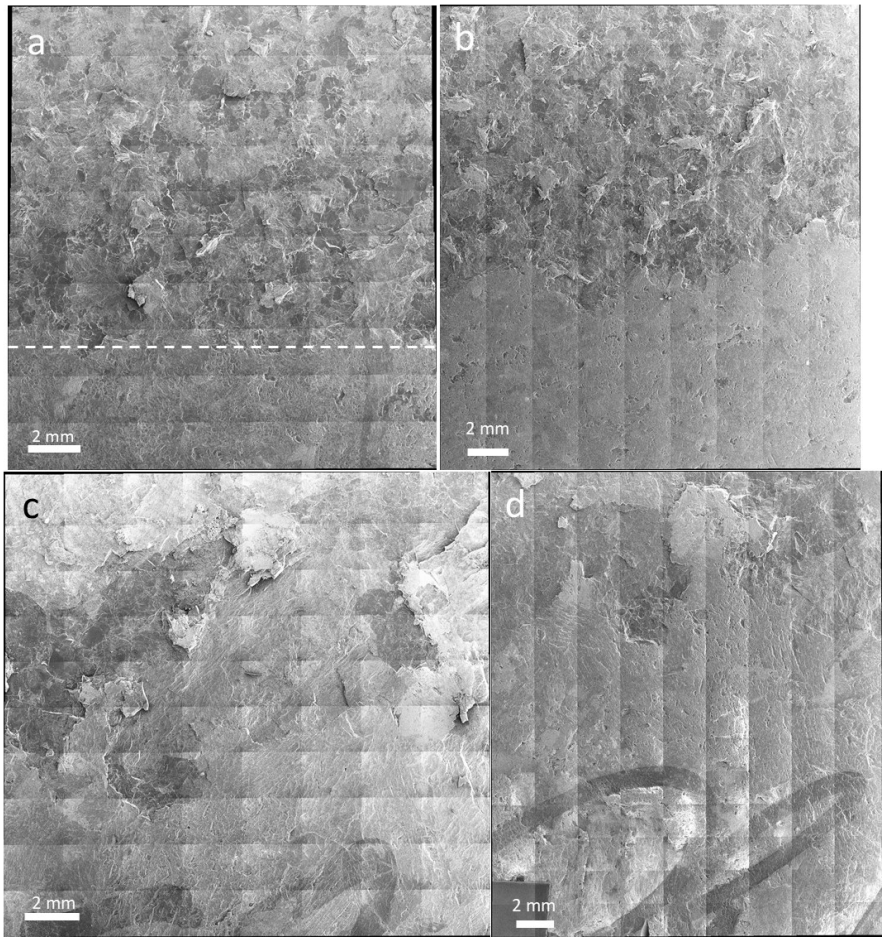

Figure 5: SEM SE image montage of plasma shocked granite samples. The path of the plasma gun was horizontal in each montage, with the exposed area at the top. (a) Kuru Grey plasma shocked 50. The white line indicates approximately the edge of the exposed area. (b) Kuru Grey plasma shocked 100 (c) Balmoral Red plasma shocked 50 (d) Balmoral Red plasma shocked 100.

3.3 µ-CT

µ-CT allows us to look inside the samples non-destructively. This allows us to study the depth of the damage caused by the thermal loading. However, the resolution depends on the distance between the X-ray source and the sample. A smaller sample therefore gives better resolution. The samples were therefore machined into smaller dimensions before µ-CT.

µ-CT cross sections of granite samples exposed to a flame torch for 60 s are shown in Figure 7. The exposed surface is at the bottom in these cross sections. In the Kuru Grey granite, the µ-CT did not resolve any damage extending into the sample. In the Balmoral Red granite, a small number of thin cracks could be seen extending several millimetres below the exposed surface. These were not seen at the other, unexposed, surfaces. These cracks could be related to the increased drillability of the Balmoral Red granite.

Figure 8 shows µ-CT images looking down at the flame torched surface. The two-dimensional cross sections show the distribution of surface pores in the flame torched Kuru Grey granite, while a few surface cracks are barely visible in the Balmoral Red granite.

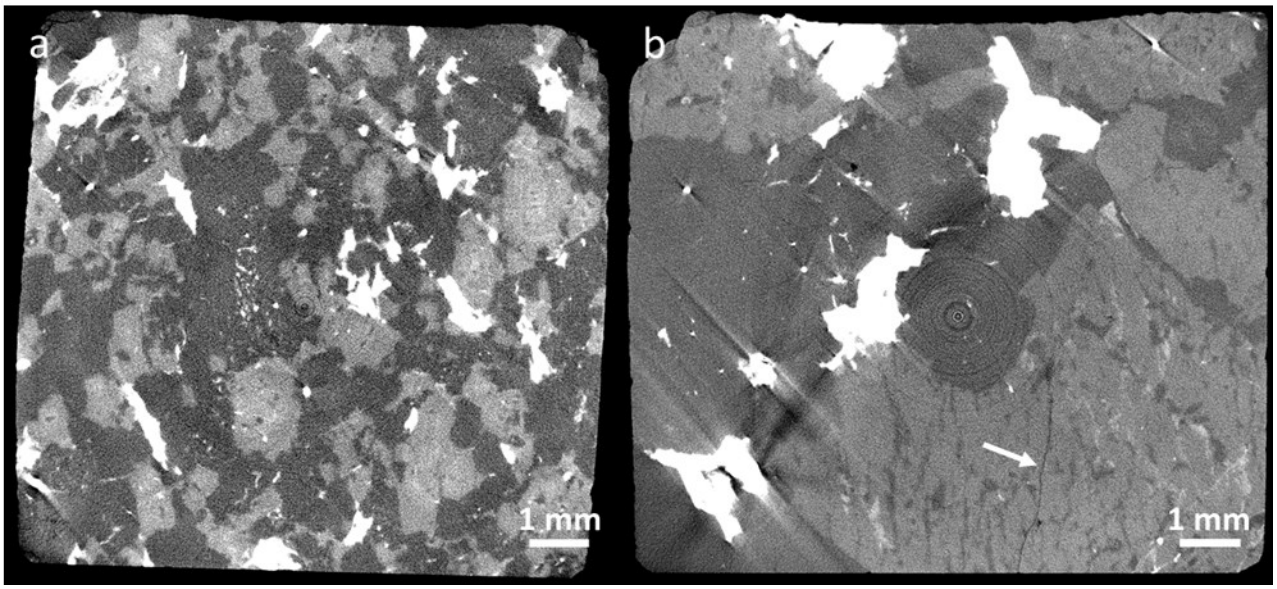

Figure 7: µ-CT cross sections of (a) Kuru Grey granite and (b) Balmoral Red granite exposed to a flame torch for 60 s. The exposed surface is at the bottom of the images. The bright iron-rich mica grains cause some streaking. A thin crack in the Balmoral Red granite is indicated by an arrow.

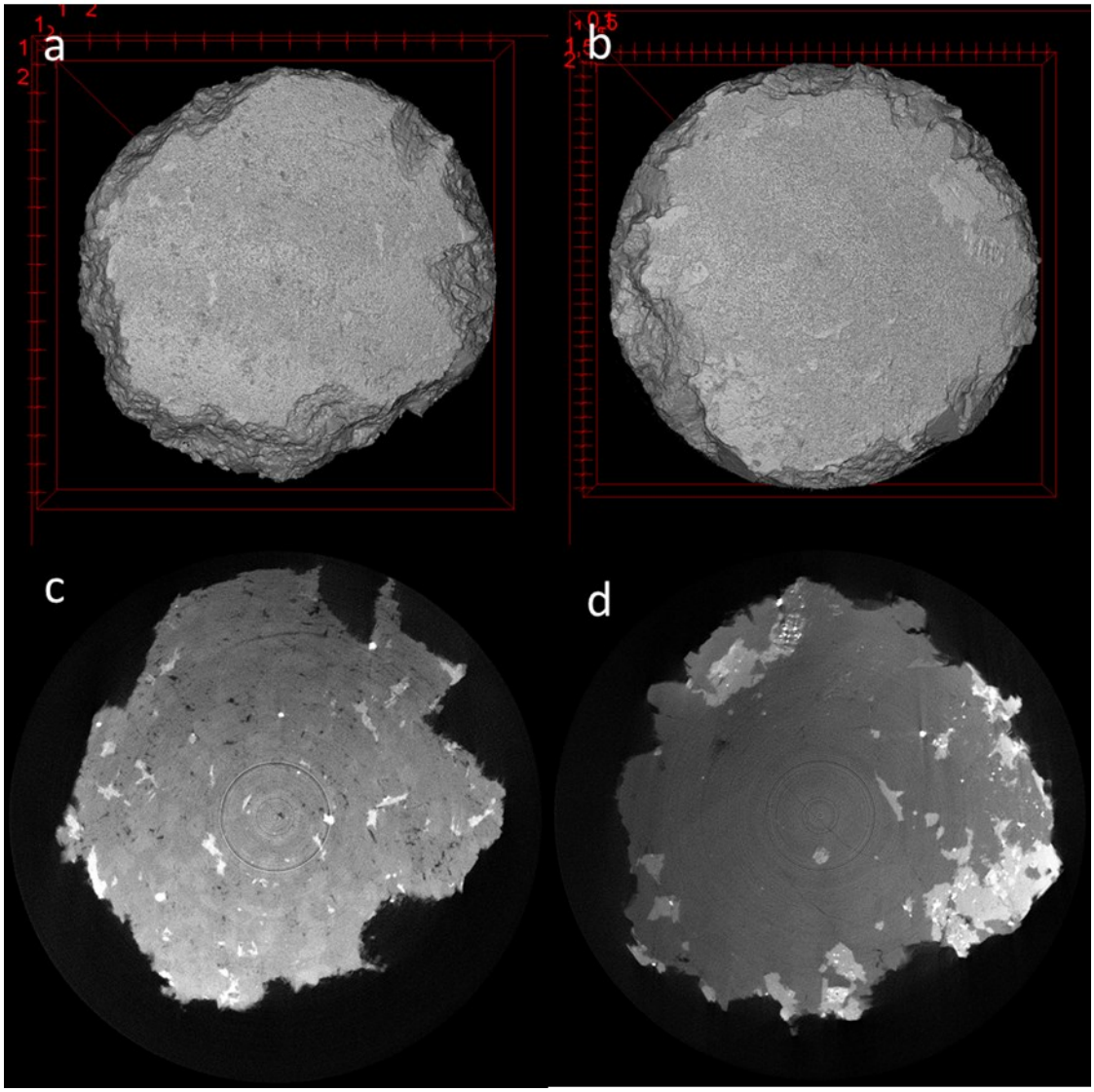

Figure 8: µ-CT data from 15 mm diameter cylinders taken from a Kuru Grey (a,c) and Balmoral Red (b,d) sample flame torched for 60 s. Top: 3D shaded models of the exposed surface. Bottom: 2D cross section of the exposed surface.

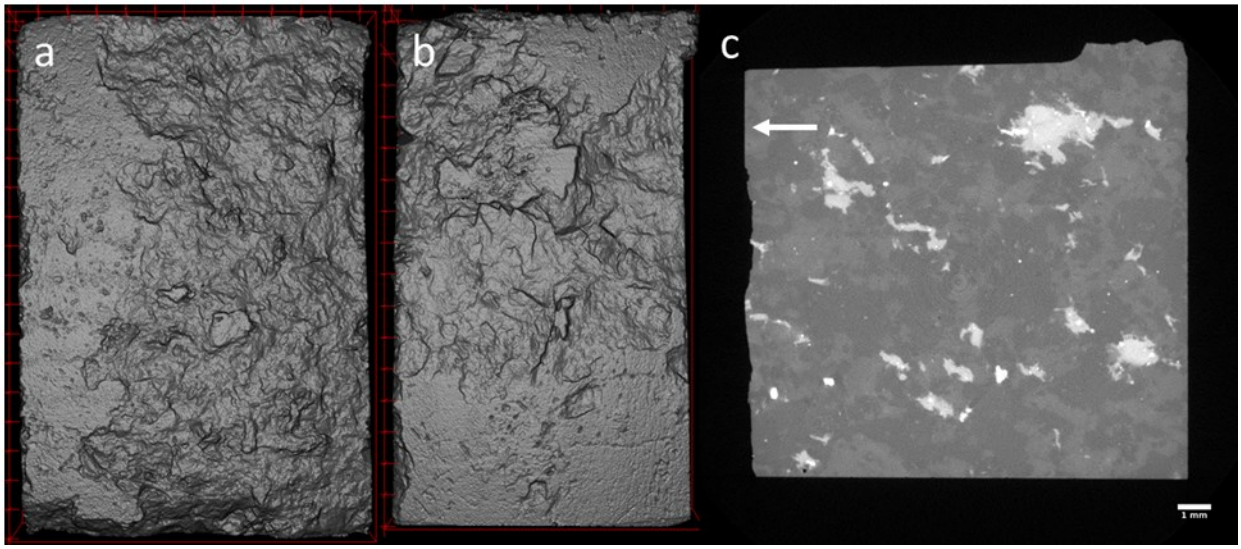

Figure 9: (a, b) µ-CT 3D shaded models of plasma shocked 100 Kuru Grey granite and plasma shocked 100 Balmoral Red granite, respectively. Unexposed rock is found in the left part of (a), and the bottom part of (b). (c) Cross-section view of the sample in (a), with the exposed surface on the left side. The unexposed part of the surface is indicated with a white arrow.

3D shaded models of the spalled surface of 2 plasma shocked samples are shown in Figure 9a,b). These images show better the rough surface created through the plasma shock treatment. A cross-section view of the plasma shocked 100 Kuru Grey sample in Figure 9c) shows that the depth of the spalling is on the order of a few hundred micrometres.

4. CONCLUSION

The Kuru Grey granite and Balmoral Red granite differed in how they responded to exposure to the stationary flame torch. The Kuru Grey showed mainly an increase in surface porosity, while large cracks were found in the Balmoral Red after exposure. The Kuru Grey granite was not weakened by the flame torch according to the miniature drill test. On the other hand, the Balmoral Red granite was significantly weakened by the flame torch in the central part of the sample which received the most heat input. Some cracks could be resolved by μ-CT, but these are likely not numerous enough to explain the large increase in the drillability of the Balmoral Red granite.

The plasma shock treatment increased the drillability in a surface layer with a thickness of a few hundred micrometres, for both the Kuru Grey and the Balmoral Red granite. This was related to the spallation of the granite surface down to a similar depth. For the Balmoral Red granite, we observe a significant increase in drillability when the plasma gun speed decreases from 75 mm/s to 50 mm/s. This could indicate a critical threshold for heat exposure to significantly soften the rock.

The plasma shock treatment reduced the scatter in the ROP in the first 100-200 μm. This is likely due to the roughness created by the thermal spallation, which reduced the effect of heterogeneities in the rock. The damage layer thickness is similar to the cutting depth in rotary drilling.

ACKNOWLEDGEMENTS

Support through the project "INNO-Drill" funded by the Research Council of Norway's ENERGIX programme (project no. 254984) is gratefully acknowledged.

REFERENCES

Dahl F, Grøv E, Breivik T (2007) Development of a new direct test method for estimating cutter life, based on the Sievers' J miniature drill test. Tunn Undergr Sp Technol 22:106–116. doi: 10.1016/j.tust.2006.03.001

Fourmeau M, Gomon D, Vacher R, et al (2014) Application of DIC Technique for Studies of Kuru Granite Rock under Static and Dynamic Loading. Procedia Mater Sci 3:691–697. doi: 10.1016/j.mspro.2014.06.114

Hood M (1976) Cutting strong rock with a drag bit assisted by high-pressure water jets. J South African Inst Min Metall 77:79–90. doi: 10.1016/0148-9062(77)91119-6

Mardoukhi A, Hokka M, Kuokkala V (2018) Experimental study of the dynamic indentation damage in thermally shocked granite. Raken Mek 51:10–26

Mardoukhi A, Mardoukhi Y, Hokka M, Kuokkala V-T (2017a) Effects of strain rate and surface cracks on the mechanical behaviour of Balmoral Red granite. Philos Trans R Soc A Math Phys Eng Sci 375:. doi: 10.1098/rsta.2016.0179

Mardoukhi A, Mardoukhi Y, Hokka M, Kuokkala V-T (2017b) Effects of Heat Shock on the Dynamic Tensile Behavior of Granitic Rocks. Rock Mech Rock Eng 50:1171–1182. doi: 10.1007/s00603-017-1168-4

Mardoukhi A, Saksala T, Hokka M, Kuokkala V-T (2017c) A numerical and experimental study on the tensile behavior of plasma shocked granite under dynamic loading. Raken Mek 50:41. doi: 10.23998/rm.65301

Rauenzahn RM, Tester JW (1989) Rock failure mechanisms of flame-jet thermal spallation drilling—theory and experimental testing. Int J Rock Mech Min Sci Geomech Abstr 26:381–399. doi: 10.1016/0148-9062(89)90935-2

Sievers H (1950) Die Bestimmung des Bohrwiderstandes von Gesteinen. Glückauf 86:776–784

Tomac I, Sauter M (2018) A review on challenges in the assessment of geomechanical rock performance for deep geothermal reservoir development. Renew Sustain Energy Rev 82:3972–3980. doi: 10.1016/j.rser.2017.10.076